1.25 mM NaH_2PO_4, 1 mM $CaCl_2$, 1 mM $MgCl_2$, 26 mM $NaHCO_3$ and 10 mM dextrose, bubbled with 95% O_2/5% CO_2 (pH 7.4). Slices (300–400 μm thick) were prepared with a vibratome (Pelco), placed in warm dissection buffer (33–35 °C) for <30 min, transferred to a holding chamber containing artificial cerebrospinal fluid (ACSF: 124 mM NaCl, 2 mM KCl, 1.5 mM $MgSO_4$, 1.25 mM NaH_2PO_4, 2.5 mM $CaCl_2$, 26 mM $NaHCO_3$, 10 mM dextrose), and kept at 22–24°C for >1 h before use. For experiments, slices were transferred to the recording chamber and perfused (4.0–4.5 ml min^{-1}) with oxygenated ACSF at 22–24 °C.

Electrophysiology

Somatic and dendritic whole-cell recordings were made in current-clamp with an Axopatch 200B amplifier (Axon) using infrared differential interference optics (IR-DIC) video microscopy. Layer 2/3 pyramidal cells were selected based on morphological and electrophysiological criteria[12,14]. Patch pipettes (somatic: 3–8 MΩ; dendritic: 8–20 MΩ) were filled with intracellular solution (120 mM K-gluconate, 10 mM HEPES, 0.1 mM EGTA, 20 mM KCl, 2 mM $MgCl_2$, 10 mM phosphocreatine, 2 mM ATP, and 0.25 mM GTP). The mean resting potential was -70.3 ± 0.7 mV, corrected for the measured liquid junction potential (6.8 mV). The series resistance was 14.6 ± 1.6 MΩ. Input resistance ($R_i = 118.0 \pm 5.4$ MΩ) was monitored with hyperpolarizing current pulses (50 pA, 100 ms); cells were excluded if R_i changed >30% over the entire experiment[12,14]. Data were filtered at 2 kHz, digitized at 10 kHz and analysed with Clampfit 8 (Axon). EPSPs were evoked by focal extracellular stimulation (0.01–1 ms, 1–100 V) with small glass bipolar electrodes. To ensure that the distal (>100 μm from soma) and proximal (<50 μm) electrodes activated separate synapses, we tested both the linear summation of EPSPs (Fig. 1b) and paired-pulse depression between inputs. Although consecutive stimulation through the same electrode induced marked paired-pulse depression of these synapses, no depression was induced by sequential stimulation through the two electrodes, indicating that they activated separate synapses. Postsynaptic APs were elicited either with depolarizing current injection through the recording electrode (1 nA, 1–4 ms; somatic recordings) or antidromically with an extracellular stimulating electrode near the axonal initial segment (0.01–1 ms, 5–100 V; dendritic recordings). Presynaptic spike timing was defined as the onset of EPSP and postsynaptic spike timing was measured at the AP peak[12,14]. Synaptic strength was measured as the initial slope (first 2 ms) of the EPSP. To measure long-term synaptic modification, a stable baseline of synaptic strength was first established by 6–12 min of recording with presynaptic stimulation at 0.2 Hz. Synaptic strength after induction was measured 11–20 min after the end of induction. For iontophoretic application of glutamate, a sharp microelectrode (150–200 MΩ) filled with 250 mM Na^+-glutamate was positioned near the apical dendrite (<5 μm). Both the holding current (1–10 nA) and ejection current (100–300 nA, 0.01–3 ms) were applied with an amplifier (Getting)[3].

Model simulation

The model consisted of one postsynaptic neuron and 100 presynaptic inputs (50 to the proximal and 50 to the distal dendrite, see diagram in Fig. 5b). The presynaptic neurons had a range of response time courses (Fig. 5a) but they were all driven by the same sensory stimulus, which was a temporally varying random signal (see Supplementary Fig. 6a). The spike train of the postsynaptic cell was simulated after integrating the synaptic input to both the distal and proximal dendritic compartments. All connection weights were initialized to 0.5 plus a small random number (Fig. 5b, upper panel), and were modified according to the STDP windows measured experimentally. Details of the model are given in Supplementary Methods.

Received 11 May; accepted 23 December 2004; doi:10.1038/nature03366.

1. Stuart, G. & Spruston, N. Determinants of voltage attenuation in neocortical pyramidal neuron dendrites. *J. Neurosci.* **18,** 3501–3510 (1998).
2. Larkum, M. E., Zhu, J. J. & Sakmann, B. A new cellular mechanism for coupling inputs arriving at different cortical layers. *Nature* **398,** 338–341 (1999).
3. Cash, S. & Yuste, R. Linear summation of excitatory inputs by CA1 pyramidal neurons. *Neuron* **22,** 383–394 (1999).
4. Magee, J. C. Dendritic integration of excitatory synaptic input. *Nature Rev. Neurosci.* **1,** 181–190 (2000).
5. Segev, I. & London, M. Untangling dendrites with quantitative models. *Science* **290,** 744–750 (2000).
6. Hausser, M., Major, G. & Stuart, G. J. Differential shunting of EPSPs by action potentials. *Science* **291,** 138–141 (2001).
7. Tamas, G., Szabadics, J. & Somogyi, P. Cell type- and subcellular position-dependent summation of unitary postsynaptic potentials in neocortical neurons. *J. Neurosci.* **22,** 740–747 (2002).
8. Hausser, M. & Mel, B. Dendrites: bug or feature? *Curr. Opin. Neurobiol.* **13,** 372–383 (2003).
9. Magee, J. C. & Johnston, D. A. synaptically controlled, associative signal for Hebbian plasticity in hippocampal neurons. *Science* **275,** 209–213 (1997).
10. Markram, H., Lubke, J., Frotscher, M. & Sakmann, B. Regulation of synaptic efficacy by coincidence of postsynaptic APs and EPSPs. *Science* **275,** 213–215 (1997).
11. Sourdet, V. & Debanne, D. The role of dendritic filtering in associative long-term synaptic plasticity. *Learn. Mem.* **6,** 422–447 (1999).
12. Feldman, D. E. Timing-based LTP and LTD at vertical inputs to layer II/III pyramidal cells in rat barrel cortex. *Neuron* **27,** 45–56 (2000).
13. Bi, G. & Poo, M. Synaptic modification by correlated activity: Hebb's postulate revisited. *Annu. Rev. Neurosci.* **24,** 139–166 (2001).
14. Froemke, R. C. & Dan, Y. Spike-timing-dependent synaptic modification induced by natural spike trains. *Nature* **416,** 433–438 (2002).
15. Watanabe, S., Hoffman, D. A., Migliore, M. & Johnston, D. Dendritic K+ channels contribute to spike-timing dependent long-term potentiation in hippocampal pyramidal neurons. *Proc. Natl Acad. Sci. USA* **99,** 8366–8371 (2002).
16. Sjostrom, P. J., Turrigiano, G. G. & Nelson, S. B. Neocortical LTD via coincident activation of presynaptic NMDA and cannabinoid receptors. *Neuron* **39,** 641–654 (2003).
17. Johnston, D. *et al.* Active dendrites, potassium channels and synaptic plasticity. *Phil. Trans. R. Soc. Lond. B Biol. Sci.* **358,** 667–674 (2003).
18. Stuart, G. J. & Hausser, M. Dendritic coincidence detection of EPSPs and action potentials. *Nature Neurosci.* **4,** 63–71 (2001).
19. Golding, N. L., Staff, N. P. & Spruston, N. Dendritic spikes as a mechanism for cooperative long-term potentiation. *Nature* **418,** 326–331 (2002).
20. Svoboda, K., Helmchen, F., Denk, W. & Tank, D. W. Spread of dendritic excitation in layer 2/3 pyramidal neurons in rat barrel cortex *in vivo*. *Nature Neurosci.* **2,** 65–73 (1999).
21. Waters, J., Larkum, M., Sakmann, B. & Helmchen, F. Supralinear Ca^{2+} influx into dendritic tufts of layer 2/3 neocortical pyramidal neurons *in vitro* and *in vivo*. *J. Neurosci.* **22,** 8558–8567 (2003).
22. Koester, H. J. & Sakmann, B. Calcium dynamics in single spines during coincident pre- and postsynaptic activity depend on relative timing of back-propagating action potentials and subthreshold excitatory postsynaptic potentials. *Proc. Natl Acad. Sci. USA* **95,** 9596–9601 (1998).
23. Zilberter, Y., Kaiser, K. M. & Sakmann, B. Dendritic GABA release depresses excitatory transmission between layer 2/3 pyramidal and bitufted neurons in rat neocortex. *Neuron* **24,** 979–988 (1999).
24. Rosenmund, C., Feltz, A. & Westbrook, G. L. Calcium-dependent inactivation of synaptic NMDA receptors in hippocampal neurons. *J. Neurophysiol.* **73,** 427–430 (1995).
25. Tong, G., Shepherd, D. & Jahr, C. E. Synaptic desensitization of NMDA receptors by calcineurin. *Science* **267,** 1510–1512 (1995).
26. Umemiya, M., Chen, N., Raymond, L. A. & Murphy, T. H. A calcium-dependent feedback mechanism participates in shaping single NMDA miniature EPSCs. *J. Neurosci.* **21,** 1–9 (2001).
27. Zucker, R. S. Calcium- and activity-dependent synaptic plasticity. *Curr. Opin. Neurobiol.* **9,** 305–313 (1999).
28. Nevian, T. & Sakmann, B. Single spine Ca^{2+} signals evoked by coincident EPSPs and backpropagating action potentials in spiny stellate cells of layer 4 in the juvenile rat somatosensory barrel cortex. *J. Neurosci.* **24,** 1689–1699 (2004).
29. Song, S., Miller, K. D. & Abbott, L. F. Competitive Hebbian learning through spike-timing-dependent synaptic plasticity. *Nature Neurosci.* **3,** 919–926 (2000).
30. Archie, K. A. & Mel, B. W. A model for intradendritic computation of binocular disparity. *Nature Neurosci.* **3,** 54–63 (2000).

Supplementary Information accompanies the paper on **www.nature.com/nature**.

Acknowledgements We thank P. Ascher, G. Bi, L. Chen, M. Frerking, E. Isacoff, R. Kramer and R. Zucker for helpful discussions, and K. Arendt, K. Borges, N. Caporale and C. Nam for technical assistance. This work was supported by grants from the National Eye Institute and the Grass Foundation. R.C.F. is a recipient of the Howard Hughes Predoctoral Fellowship.

Competing interests statement The authors declare that they have no competing financial interests.

Correspondence and requests for materials should be addressed to Y.D. (ydan@berkeley.edu).

The receptors and coding logic for bitter taste

Ken L. Mueller[1], Mark A. Hoon[2], Isolde Erlenbach[2], Jayaram Chandrashekar[1], Charles S. Zuker[1] & Nicholas J. P. Ryba[2]

[1]*Howard Hughes Medical Institute and Departments of Biology and Neurosciences, University of California at San Diego, La Jolla, California 92093-0649, USA*
[2]*National Institute of Dental and Craniofacial Research, National Institutes of Health, Bethesda, Maryland 20892, USA*

The sense of taste provides animals with valuable information about the nature and quality of food. Bitter taste detection functions as an important sensory input to warn against the ingestion of toxic and noxious substances. T2Rs are a family of approximately 30 highly divergent G-protein-coupled receptors (GPCRs)[1,2] that are selectively expressed in the tongue and palate epithelium[1] and are implicated in bitter taste sensing[1–8]. Here we demonstrate, using a combination of genetic, behavioural and physiological studies, that T2R receptors are necessary and sufficient for the detection and perception of bitter compounds, and show that differences in T2Rs between species (human and mouse) can determine the selectivity of bitter taste responses. In addition, we show that mice engineered to express a bitter taste

receptor in 'sweet cells'[9] become strongly attracted to its cognate bitter tastants, whereas expression of the same receptor (or even a novel GPCR) in T2R-expressing cells resulted in mice that are averse to the respective compounds. Together these results illustrate the fundamental principle of bitter taste coding at the periphery: dedicated cells act as broadly tuned bitter sensors that are wired to mediate behavioural aversion.

Two main lines of evidence suggest that T2Rs function as mammalian bitter taste receptors. First, heterologous expression assays have shown that several human and rodent T2Rs respond to bitter tasting compounds: mouse (m)T2R5 is a high affinity receptor for cycloheximide (Cyx)[3], human (h)T2R16 is a candidate receptor for β-glucopyranosides (salicin and related compounds)[4], hT2R14 is a candidate receptor for picrotoxinin[6], and hT2R44 and hT2R61/hT2R43 are receptors for denatonium, aristolochic acid and 6-nitrosaccharin[7,8]. Second, sequence polymorphisms in T2Rs have been linked to differences in bitter taste sensitivity in mice[3] and humans[5]. To determine if T2Rs and T2R-expressing cells are necessary and sufficient for bitter taste perception *in vivo*, we used several complementary strategies. First, we genetically engineered mice to express candidate human T2R receptors for tastants that mice do not respond to, and examined whether introduction of these candidate bitter receptors endows the animals with an expanded bitter taste repertoire. Second, we generated genetically modified mice lacking a specific T2R and studied their behavioural and physiological responses to bitter compounds. Third, we examined the specificity of bitter taste responses of animals in which all sweet, umami and bitter taste function was eliminated and then selectively restored in T2R-expressing cells. Finally, we functionally dissected the role of cells and receptors by ectopically expressing a T2R bitter taste receptor in sweet-sensing[9] (T1R) cells.

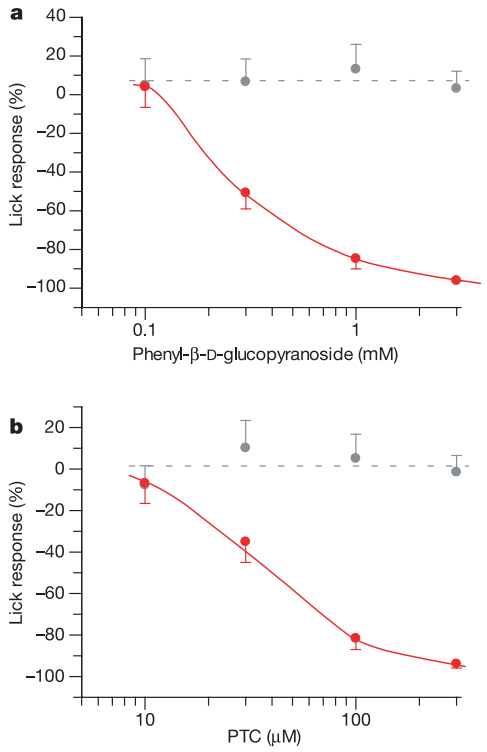

Figure 1 Introduction of human bitter receptors expands the bitter taste repertoire of mice. Brief-access taste tests measuring immediate lick responses show that normal FVB/N mice, unlike humans[4,5], do not taste phenyl-β-D-glucopyranoside or PTC (grey). In contrast, transgenic mice expressing the human T2R taste receptors for phenyl-β-D-glucopyranoside or PTC in bitter-sensing cells show robust behavioural aversion to these tastants (red). **a**, Mice expressing the human T2R16 taste receptor under the control of the mT2R19 promoter (red) respond to concentrations of phenyl-β-D-glucopyranoside that taste bitter to humans. **b**, Transgenic mice expressing human T2R38 (red) are averse to PTC at concentrations closely mimicking human sensitivity to this tastant. These mice respond normally to control bitter compounds (data not shown). Values are means ± s.e.m. ($n = 8$).

Mice and humans have distinctive differences in their sensitivities to many bitter compounds. For example, several β-glucopyranosides evoke strong bitter taste in humans, yet mice are largely indifferent to these compounds. Similarly, phenylthiocarbamide (PTC), a well known bitter tastant often used in human genetic studies, is ineffective in mice (Fig. 1). We placed the candidate human receptor for β-glucopyranosides (hT2R16, ref. 4) and PTC (hT2R38, ref. 5) under the control of a mouse T2R promoter[1,10], and generated transgenic animals expressing either of these two candidate taste receptors in T2R-expressing cells. To examine taste behaviour, we measured taste choices in two-bottle intake preference assays, or by direct counting of immediate licking responses in a multi-channel gustometer (see Methods and ref. 10). Figure 1 shows that T2R-hT2R16 transgenic animals acquire the ability to detect and respond to phenyl-β-D-glucopyranoside at concentrations that closely approximate the human physiological taste sensitivity range[4]. Likewise, expression of hT2R38 confers selective PTC sensitivity to the engineered mice. These results validate T2Rs and T2R-expressing cells as mediators of bitter taste perception *in vivo*, and demonstrate that T2Rs are sufficient for selective responses to bitter tastants; they also confirm that hT2R16 is the β-glucopyranoside receptor[4] and hT2R38 is the PTC receptor[5]. In addition, the ability to confer human bitter taste responses on mice by introduction of human taste receptors illustrates an important feature of T2Rs and bitter taste: selectivity and sensitivity differences to bitter compounds between species is probably a reflection of sequence differences in the respective T2R repertoires.

Next, we used homologous recombination to generate animals lacking mT2R5, the candidate Cyx receptor[3]. If T2R5 is the principal bitter taste receptor for Cyx, then its knockout should abolish most, if not all, responses to cycloheximide. To explore the effect of this knockout *in vivo*, we recorded tastant-induced action potentials from one of the principal nerves innervating taste receptor cells of the tongue. Figure 2 shows that T2R5$^{-/-}$ mice have a dramatic and selective loss of responses to Cyx. In addition, the animals are no longer behaviourally averse to Cyx, even at concentrations 100-fold higher than those required to trigger strong repulsion in wild-type mice. As expected, responses to sweet, umami, sour and salty tastants are physiologically and behaviourally comparable to controls. To further examine the taste repertoire of the T2R5$^{-/-}$ mice, we performed studies of bitter taste against a broad panel of bitter tastants. T2R5$^{-/-}$ animals retain basically normal responses to all other bitter tastants tested (Fig. 2 and Supplementary Fig. 2). These results prove the essential requirement of a T2R receptor for bitter taste, and together with our T2R mis-expression studies (Fig. 1) show that defined T2Rs are both necessary and sufficient for bitter taste sensation. Interestingly, T2R5$^{-/-}$ mice show residual responses to millimolar levels of cycloheximide, but mice defective in all bitter taste signalling (for example, phospholipase C β2 knockout (PLCβ2$^{-/-}$) mice, ref. 10) have a complete loss of Cyx sensitivity (Fig. 2b); we suggest that this residual activity in T2R5$^{-/-}$ mice reflects the recruitment of lower affinity T2Rs.

Previously, we showed that most T2R receptor genes are co-expressed in the same subset of taste receptor cells of the tongue and palate epithelium[1]. We interpreted this to mean that individual T2R-expressing cells act as broadly tuned bitter sensors capable of responding to a wide diversity of tastants but not necessarily able to discriminate between them. Recently, we used mice deficient in sweet, umami and bitter taste (owing to a deletion of the PLCβ2 effector molecule[10]) to ask whether taste receptor cells are tuned to single or multiple taste modalities. By selectively rescuing PLCβ2

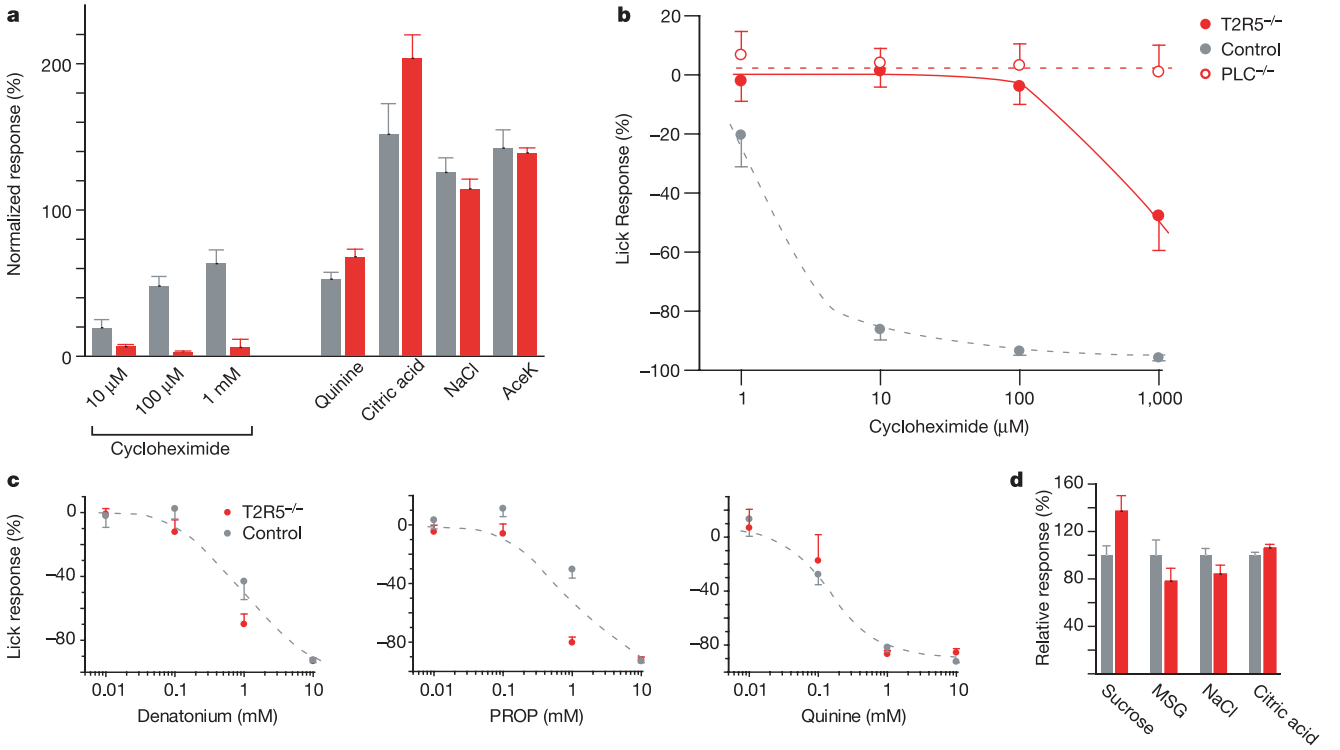

Figure 2 T2R5 is necessary for cycloheximide taste reception and perception. T2R5$^{-/-}$ mice show a strong and selective impairment in their ability to taste cycloheximide. **a**, Electrophysiological responses to cycloheximide are essentially eliminated in knockout mice (red bars), but responses to other tastants are equivalent to those of control animals[10] (grey bars; see Supplementary Information). Shown are integrated chorda tympani responses normalized to the response to 100 mM NH_4Cl (ref. 21). T2R5$^{-/-}$ mice show a severe selective deficit in their ability to taste cycloheximide (**b**) but not to other bitter (**c**) or sweet, umami, salty or sour tastants (**d**). **b**, At concentrations 100-fold higher than those needed to trigger maximal aversion in control animals, T2R5$^{-/-}$ mice begin to show behavioural aversion. This probably reflects the recruitment of a low-sensitivity receptor for cycloheximide; total ablation of the bitter taste system (for example, PLCβ2$^{-/-}$ animals; open circles) eliminates this residual response. Values are means ± s.e.m.; $n = 3$ (**a**), $n = 8$ (**b**–**d**). See Supplementary Information for responses to additional tastants in T2R5$^{-/-}$ animals.

function only in T2R-expressing cells, we showed that there is complete functional segregation between attractive (sweet, umami) and aversive (bitter) tastes[10]. We now make use of a similar strategy to ask whether re-introduction of PLCβ2 under the control of selective T2R-promoters restores complete or only partial bitter taste. If indeed individual T2R-cells express most bitter taste receptors, then targeting expression of a PLCβ2 'rescue' construct under the control of any one T2R promoter should be sufficient to restore normal bitter taste (that is, if the cell can now signal, all the receptors will function). Conversely, if different T2R-expressing

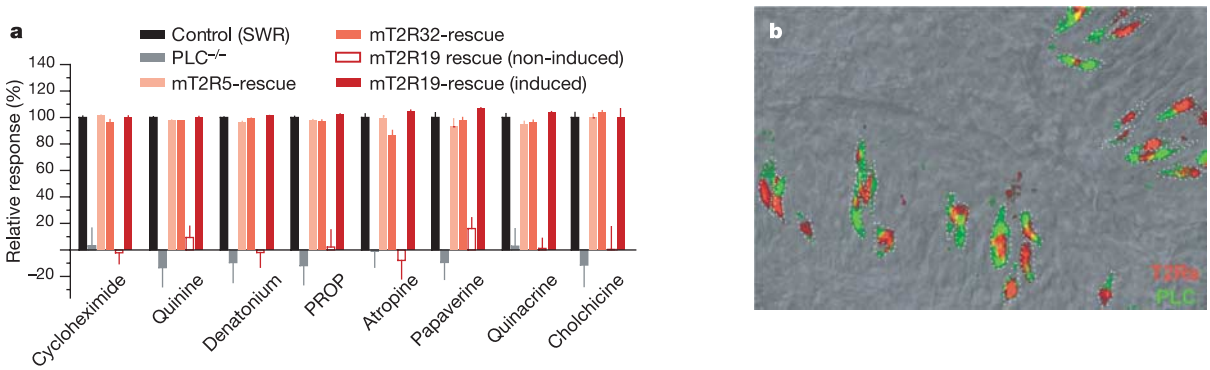

Figure 3 T2R-expressing cells are the mediators of bitter taste. **a**, Taste preferences of control (black), PLCβ2$^{-/-}$ (grey), and transgenic 'rescue' lines that express PLCβ2 under the control of mT2R5, mT2R32 or mT2R19 (shades of red) were measured relative to water using a brief-access test against a panel of bitter tastants. The rescue line mT2R19 was engineered as a two component Tet-on system[9]. In the absence of doxycycline, the mT2R19 rescue mice (open red bars) do not taste bitter compounds. PLCβ2 knockout completely eliminates bitter taste behaviour[10]. However, expression of PLCβ2 under the control of each of the three different T2R promoters restores normal bitter taste to a broad panel of chemically diverse bitter tastants; this demonstrates broadly tuned bitter sensing for the cells that express T2R5, T2R19 andT2R32, and demonstrates that a large repertoire of T2Rs is expressed in each T2R-expressing cell[1]. Values shown are means ± s.e.m. ($n = 6$–12). For additional data and tastants, see Supplementary Fig. 3 **b**, T2R regulatory sequences drive PLCβ2 expression in T2R-expressing cells. Shown is double labelling of T2R32 driving PLCβ2 expression in a PLCβ2$^{-/-}$ background, demonstrating coexpression of PLCβ2 (immunoreactivity, green) and T2Rs (*in situ* hybridization, red); dotted lines highlight taste receptor cells. The *in situ* signal is concentrated around the cell nucleus, whereas immunostaining is primarily cytoplasmic.

cells are narrowly tuned to different subsets of bitter tastants[11], then mice with restricted PLC expression would regain bitter sensitivity to a discrete repertoire of bitter-tasting compounds.

To address this question we chose three divergent T2Rs mapping to different chromosomal locations (T2R5, T2R19 and T2R32, ref. 1) and used their regulatory sequences to drive PLCβ2 expression in PLCβ2$^{-/-}$ lines. We then tested the engineered animals against a broad panel of chemically diverse bitter compounds (Fig. 3 and Supplementary Fig. 3). In addition, we designed one of the three constructs to have an inducible expression system, in order to determine whether T2R signalling plays a critical role in the development and/or connectivity of T2R cells. Remarkably, all of the PLCβ2-rescued animals showed completely normal bitter taste (Fig. 3), including those in which T2R function was restored only at the adult stage, long after the taste system would have completed its normal development and wiring programme[12]. These results show that the bitter taste circuitry can be established without bitter sensory input, and unequivocally demonstrate that individual T2R cells operate as broadly tuned bitter sensors.

Recently, we generated mice expressing a RASSL[13] κ-opioid receptor in sweet cells and showed that these animals become selectively attracted to the synthetic opioid agonist spiradoline, a normally tasteless compound[9]. Thus, activation of sweet cells, rather than the sweet taste receptor itself, results in the perception of sweetness. Does the same logic apply to bitter taste? We tested this idea by generating mice in which an inducible RASSL receptor was now targeted to bitter taste cells. Figure 4 shows that non-induced animals, or wild-type controls treated with doxycycline, are completely insensitive to the RASSL agonist spiradoline, even at millimolar concentrations. In contrast, mice expressing RASSL in bitter cells show strong aversion to spiradoline. Together, these results substantiate the coding of both sweet and bitter pathways by dedicated (that is, labelled) lines. A final corollary emerging from these findings is that expression of a sweet receptor in bitter cells should trigger behavioural aversion to sweet tastants, and expression of a bitter receptor in sweet cells should result in attraction to the bitter compound. Accordingly, we engineered mice expressing the bitter receptor for β-glucopyranosides in sweet cells. Indeed, these mice now display strong attraction to this family of bitter compounds. Thus, the 'taste' of a sweet or a bitter compound (that is, the perception of sweet and bitter) is a reflection of the selective activation of T1R-expressing versus T2R-expressing cells, rather than a property of the receptors or even the tastant molecules. □

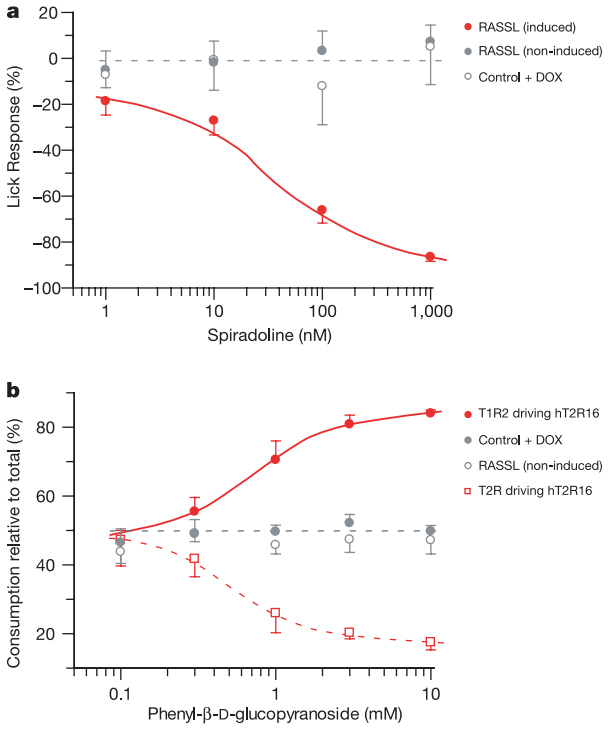

Figure 4 Switching the behavioural taste responses of mice by mis-expression of a bitter taste receptor. **a**, Expression of RASSL[13] in T2R-expressing cells generates animals that show specific behavioural aversion to spiradoline (red). No responses are seen in control mice that carry the rtTA transgene but lack the RASSL receptor (open grey circles) or in non-induced RASSL mice (filled grey circles), even at 100 times the concentration needed to elicit strong responses in RASSL-expressing animals. **b**, Transgenic mice expressing human T2R16 (under control of the mT2R19 promoter) in bitter cells show strong behavioural aversion to phenyl-β-D-glucopyranoside (open red squares). Expression of the same receptor in sweet cells (T1R2-expressing cells) generates animals that show strong attraction for this bitter tastant (filled red circles). Control animals (filled grey circles) or non-induced experimental animals (open grey circles) show no preference or aversion to this tastant. Values are means ± s.e.m. ($n = 8$).

Methods

Gene targeting of T2R5

T2R5 knockout mice were generated by homologous recombination following standard procedures[9,10]. The entire coding sequence of T2R5 was replaced by a reverse-tetracycline dependent transactivator (rtTA) and a loxP-flanked PGK-neo^r cassette (see Supplementary Fig. 1 for details). Homologous recombination in R1 embryonic stem (ES) cells was detected by diagnostic Southern hybridization with probes outside the targeting construct. Two targeted ES clones were injected into C57BL/6 blastocysts. Chimaeric mice were bred with C57BL/6 mice and progeny backcrossed to C57BL/6 mice for two generations before establishing a homozygous knockout colony.

Transgenic animals

Transgenic lines were produced by pronuclear injection of zygotes from FVB/N or CB6 (BALB/c × C57BL/6 hybrids) mice. For constructs using the Tet-on inducible system, tetracycline-dependent gene expression was induced by feeding animals a diet containing doxycycline (6 g kg^{-1}) (Bio-Serv) for 3 days before and during behavioural testing[9]. For each construct, at least two independent animal lines were generated. The T2R38 transgenic construct used the PAV-taster allele[5]. For transgenic constructs using T2R regulatory sequences, we used the following fragments: T2R5, −10816 to +3 (the location of the ATG start codon)[10]; T2R19, −11012 to +3; T2R32, −9506 to +3. *In situ* hyrbridization and immunhistochemistry were carried out as described previously[10].

Behavioural assays

Taste behaviour was assayed using a short-term assay that directly measures taste preferences by counting immediate licking responses in a multi-channel gustometer (Davis MS160-Mouse gustometer; DiLog Instruments)[14]. Before training and behavioural testing, all mice with a T2R5$^{-/-}$ or PLCβ2$^{-/-}$ background were treated with intranasal zinc sulphate[15] to reduce input through the olfactory system. Mice were trained and tested as described previously[9,10]. Salt attraction to 150 mM NaCl was measured in mice that had been salt deprived overnight[16]. Lick response represents the mean percentage rate at which mice licked a tested compound relative to their sampling of an appropriate control tastant; relative responses were scaled to the mean response of control animals. The concentrations of tastants used for bar graphs were: 300 mM sucrose; 100 mM glutamate + 1 mM inosine monophosphate +0.1 mM amiloride (MSG); 150 mM NaCl (attraction); 150 mM citric acid; 10 μM cycloheximide; 10 mM quinine; 10 mM denatonium; 10 mM 6-*n*-propyl-2-thiouracil (PROP); 10 mM papaverine; 10 mM quinacrine; 1 mM cholchicine, 5 mM atropine.

Standard two-bottle preference assays were carried out as described previously[17]. For the two-bottle assays in Fig. 4b, consumption relative to total is defined as intake of tastant divided by total intake (tastant plus water). For mice carrying rtTA and TetO-transgenes, controls included testing the same mice without induction as well as mice carrying just the rtTA transgene and exposed to doxycycline.

Nerve recordings

Lingual stimulation and recording procedures were performed as previously described[18,19]. Neural signals were amplified (5,000×) with a Grass P511 AC amplifier (Astro-Med), digitized with a Digidata 1200B A/D converter (Axon Instruments), and integrated with a time constant of 0.5 s. Taste stimuli were presented at a constant flow rate of 4 ml min^{-1} for 20 s intervals, interspersed by 2 min rinses with artificial saliva[20] between presentations. All data analyses used the integrated response over a 25 s period immediately after the application of the stimulus. The mean response to 100 mM NH_4Cl was used to normalize responses to each experimental series.

Tastants used for nerve recordings (maximal concentrations) were: 60 mM acesulfameK (AceK); 100 mM citric acid; 100 mM NaCl; 100 mM NH_4Cl; 10 mM quinine; 1 mM cycloheximide.

Received 3 December 2004; accepted 10 January 2005; doi:10.1038/nature03352.

1. Adler, E. *et al.* A novel family of mammalian taste receptors. *Cell* **100,** 693–702 (2000).
2. Matsunami, H., Montmayeur, J. P. & Buck, L. B. A family of candidate taste receptors in human and mouse. *Nature* **404,** 601–604 (2000).
3. Chandrashekar, J. *et al.* T2Rs function as bitter taste receptors. *Cell* **100,** 703–711 (2000).
4. Bufe, B., Hofmann, T., Krautwurst, D., Raguse, J. D. & Meyerhof, W. The human TAS2R16 receptor mediates bitter taste in response to beta-glucopyranosides. *Nature Genet.* **32,** 397–401 (2002).
5. Kim, U. K. *et al.* Positional cloning of the human quantitative trait locus underlying taste sensitivity to phenylthiocarbamide. *Science* **299,** 1221–1225 (2003).
6. Behrens, M. *et al.* The human taste receptor hTAS2R14 responds to a variety of different bitter compounds. *Biochem. Biophys. Res. Commun.* **319,** 479–485 (2004).
7. Pronin, A. N., Tang, H., Connor, J. & Keung, W. Identification of ligands for two human bitter T2R receptors. *Chem. Senses* **29,** 583–593 (2004).
8. Kuhn, C. *et al.* Bitter taste receptors for saccharin and acesulfame K. *J. Neurosci.* **24,** 10260–10265 (2004).
9. Zhao, G. Q. *et al.* The receptors for mammalian sweet and umami taste. *Cell* **115,** 255–266 (2003).
10. Zhang, Y. *et al.* Coding of sweet, bitter, and umami tastes: different receptor cells sharing similar signaling pathways. *Cell* **112,** 293–301 (2003).
11. Caicedo, A. & Roper, S. D. Taste receptor cells that discriminate between bitter stimuli. *Science* **291,** 1557–1560 (2001).
12. Farbman, A. I. Electron microscope study of the developing taste bud in rat fungiform papilla. *Dev. Biol.* **11,** 110–135 (1965).
13. Coward, P. *et al.* Controlling signaling with a specifically designed Gi-coupled receptor. *Proc. Natl Acad. Sci. USA* **95,** 352–357 (1998).
14. Glendinning, J. I., Gresack, J. & Spector, A. C. A high-throughput screening procedure for identifying mice with aberrant taste and oromotor function. *Chem. Senses* **27,** 461–474 (2002).
15. McBride, K., Slotnick, B. & Margolis, F. L. Does intranasal application of zinc sulfate produce anosmia in the mouse? An olfactometric and anatomical study. *Chem. Senses* **28,** 659–670 (2003).
16. Franchini, L. F., Rubinstein, M. & Vivas, L. Reduced sodium appetite and increased oxytocin gene expression in mutant mice lacking beta-endorphin. *Neuroscience* **121,** 875–881 (2003).
17. Nelson, G. *et al.* Mammalian sweet taste receptors. *Cell* **106,** 381–390 (2001).
18. Dahl, M., Erickson, R. P. & Simon, S. A. Neural responses to bitter compounds in rats. *Brain Res.* **756,** 22–34 (1997).
19. Nelson, G. *et al.* An amino-acid taste receptor. *Nature* **416,** 199–202 (2002).
20. Danilova, V. & Hellekant, G. Comparison of the responses of the chorda tympani and glossopharyngeal nerves to taste stimuli in C57BL/6J mice. *BMC Neurosci.* **4,** 5 (2003).
21. Nakashima, K. & Ninomiya, Y. Transduction for sweet taste of saccharin may involve both inositol 1,4,5-trisphosphate and cAMP pathways in the fungiform taste buds in C57BL mice. *Cell. Physiol. Biochem.* **9,** 90–98 (1999).

Supplementary Information accompanies the paper on **www.nature.com/nature.**

Acknowledgements We thank F. Liu for help generating T2R5 knockout animals. We are also grateful to A. Cho and S. Taduru for generation of transgenic lines, and to A. Leslie for preparation of antibodies. We thank members of the Zuker and Ryba laboratories for valuable comments and advice. This work was supported in part by a grant from the National Institute on Deafness and Other Communication Disorders to C.S.Z. C.S.Z. is an investigator of the Howard Hughes Medical Institute.

Competing interests statement The authors declare that they have no competing financial interests.

Correspondence and requests for materials should be addressed to C.S.Z. (charles@flyeye.ucsd.edu) or N.J.P.R. (nick.ryba@nih.gov).

Spatial bistability of Dpp–receptor interactions during *Drosophila* dorsal–ventral patterning

Yu-Chiun Wang[1] **& Edwin L. Ferguson**[1,2]

[1]*Department of Organismal Biology and Anatomy and* [2]*Department of Molecular Genetics and Cell Biology, University of Chicago, Chicago, Illinois 60637, USA*

In many developmental contexts, a locally produced morphogen specifies positional information by forming a concentration gradient over a field of cells[1]. However, during embryonic dorsal–ventral patterning in *Drosophila*, two members of the bone morphogenetic protein (BMP) family, Decapentaplegic (Dpp) and Screw (Scw), are broadly transcribed but promote receptor-mediated signalling in a restricted subset of expressing cells[2–4]. Here we use a novel immunostaining protocol to visualize receptor-bound BMPs and show that both proteins become localized to a sharp stripe of dorsal cells. We demonstrate that proper BMP localization involves two distinct processes. First, Dpp undergoes directed, long-range extracellular transport. Scw also undergoes long-range movement, but can do so independently of Dpp transport. Second, an intracellular positive feedback circuit promotes future ligand binding as a function of previous signalling strength. These data elicit a model in which extracellular Dpp transport initially creates a shallow gradient of BMP binding that is acted on by positive intracellular feedback to produce two stable states of BMP–receptor interactions, a spatial bistability in which BMP binding and signalling capabilities are high in dorsal-most cells and low in lateral cells.

The combined activities of both *dpp* and *scw* are necessary for phosphorylation of the BMP signal transducer Mad and ultimately for the specification of dorsal tissues in the *Drosophila* embryo[3–5]. Although *dpp* is expressed uniformly over the dorsal 40% of the embryonic circumference and *scw* is ubiquitously expressed, at the onset of gastrulation (stage 6) phosphorylated Mad (pMad) staining is restricted to the dorsal 10% of cells that comprise the extraembryonic amnioserosa[2–4] (Fig. 1c). However, the pattern of pMad staining is dynamic during development. pMad staining is initially visualized during early and mid-stage 5 as a broad, shallow gradient centred on the dorsal midline (Fig. 1a, b). Over the 30 min period between mid-stage 5 and stage 6, the intensity of pMad staining refines, decreasing laterally but significantly increasing dorsally[6,7] (Fig. 1d).

Because this pattern of BMP signalling does not result from restricted expression of BMP receptors[8–11], we determined whether it reflects region-specific ligand–receptor interaction by developing a technique, called perivitelline injection (PVI), to visualize secreted, receptor-bound Dpp. We injected anti-green fluorescent protein (GFP) antibody into the embryonic perivitelline space, the extracellular space between the cell membrane and the vitelline membrane, to detect a biologically active, GFP-tagged form[12] of Dpp expressed under control of the *even-skipped* stripe 2 (*eve-st2*) enhancer[13] (Fig. 1e). Because injected antibody does not have access to the cytoplasm, it can only interact with secreted Dpp–GFP. After fixation and removal of the vitelline membrane, only antibody bound to Dpp–GFP that is associated with the embryo will be visualized.

Using PVI, we observed that Dpp–GFP is localized to a stripe on the dorsal side of the embryo in a pattern distinctly different from that obtained by conventional immunostaining, which visualizes Dpp–GFP at its site of production, probably in the secretory pathway (Fig. 1f–h). PVI initially detects low levels of Dpp–GFP at mid-stage 5 in a broad dorsal domain centred on the *eve-st2* region (Fig. 1g). By early stage 6, a narrow stripe of Dpp–GFP, which extends over the entire anterior–posterior length of the embryo (Fig. 1h), closely mirrors the spatial extent of pMad staining (Fig. 1j). The immunofluorescence appears to be associated with cell membranes and in punctate structures within cells (Fig. 1i), representing Dpp–GFP bound to the cell surface or internalized, presumably in association with its receptor. The ability to detect the dorsal stripe of Dpp–GFP with conventional immunostaining after PVI (Fig. 1k) suggests that PVI stabilizes an otherwise transient process of ligand–receptor interaction and endocytic processing. Using PVI, we confirmed that an HA-tagged form of Dpp expressed in its endogenous domain also localizes dorsally (Fig. 1l). These findings demonstrate that Dpp undergoes long-range, directional extracellular transport to become localized to the dorsal-most cells.

Two secreted proteins, the ventro-laterally expressed Short gastrulation (Sog) and the dorsally expressed Twisted gastrulation (Tsg), form a tripartite complex with Dpp that blocks Dpp–receptor